Nucleic Acids Research, 2025, **53**, gkaf073
https://doi.org/10.1093/nar/gkaf073
Genome integrity, repair and replication

Mono-ubiquitination of TopBP1 by PHRF1 enhances ATR activation and genomic stability

Fei Zhao[1], Chenghui Cai[1], Huanyao Gao[2], Jaeyoung Moon[3], Grania Christyani[3], Sisi Qin[3], Yalan Hao[4], Tongzheng Liu[5], Zhenkun Lou[2,*], Wootae Kim[3,*]

[1]College of Biology, Hunan University, Changsha 410082, China
[2]Department of Molecular Pharmacology and Experimental Therapeutics, Mayo Clinic, Rochester, MN 55905, United States
[3]Department of Integrated Biomedical Science, Soonchunhyang Institute of Medi-bio Science (SIMS), Soonchunhyang University, Cheonan 31151 Chungcheongnam-do, Republic of Korea
[4]Analytical Instrumentation Center, Hunan University, Changsha 410082, China
[5]College of Pharmacy/International Cooperative Laboratory of Traditional Chinese Medicine Modernization and Innovative Drug Development of Ministry of Education (MOE) of China, Jinan University, Guangzhou 510632, China

[*]To whom correspondence should be addressed. Email: wootaek@sch.ac.kr
Correspondence may also be addressed to Zhenkun Lou. Email: lou.zhenkun@mayo.edu

Abstract

The TopBP1-ATR axis is critical for maintaining genomic stability during DNA replication stress, yet the precise regulation of TopBP1 in replication stress responses remains poorly understood. In this study, we identified PHD and Ring Finger Domains 1 (PHRF1) as an important ATR activator through its interaction with TopBP1. Our analysis revealed a correlation between PHRF1 and genomic stability in cancer patients. Mechanistically, PHRF1 is recruited to DNA lesions in a manner dependent on its PHD domain and histone methylation. Subsequently, PHRF1 mono-ubiquitinates TopBP1 at lysine 73, which enhances the TopBP1-ATR interaction and activates ATR. Depletion of PHRF1 disrupts ATR activation and sensitizes cells to replication stress-inducing agents. Furthermore, conditional knockout of *Phrf1* in mice leads to early lethality and impaired ATR-Chk1 axis signaling. Collectively, our findings establish PHRF1 as a novel E3 ligase for TopBP1, coordinating the replication stress response by enhancing TopBP1-ATR signaling.

Graphical abstract

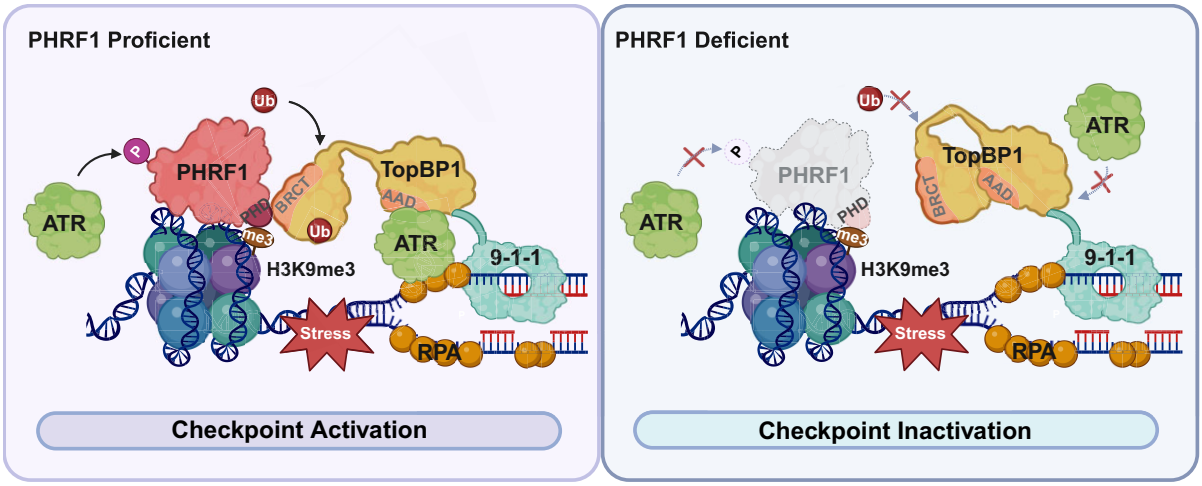

Introduction

DNA replication is a finely tuned and tightly regulated process essential for the accurate duplication of the genome. However, this process is constantly exposed to both endogenous and exogenous stressors that can stall replication forks, resulting in the accumulation of DNA damage. If not properly resolved, such replication stress can lead to mutations, chromosomal aberrations, and ultimately, genome instability, a hallmark of various human diseases, including cancer [1, 2]. To counteract these threats, eukaryotic cells have evolved a sophisticated

Received: March 12, 2024. **Revised:** December 28, 2024. **Editorial Decision:** January 20, 2025. **Accepted:** January 28, 2025

DNA damage response (DDR) network that safeguards genomic stability by orchestrating the detection, signaling, and repair of DNA lesions [3, 4].

Central to the cellular response to replication stress is the ATR-TopBP1-Chk1 axis, an essential signaling pathway activated in response to replication fork stalling. ATR (ataxia telangiectasia and Rad3-related) kinase, recruited and activated by TopBP1 (topoisomerase II binding protein 1), plays a pivotal role in stabilizing and restarting stalled replication forks, preventing fork collapse, and facilitating cell cycle progression [5–9]. Activation of ATR is initiated when single-stranded DNA (ssDNA) generated at stalled forks is rapidly coated by replication protein A (RPA), forming an RPA–ssDNA complex that serves as a platform for the recruitment of key factors, including ATR-ATRIP, the Rad17-RFC-9–1-1 complex, and ETAA1 [8, 10–15]. The assembly and activation of this signaling cascade are highly regulated by post-translational modifications (PTMs), such as phosphorylation and ubiquitination, which fine-tune the functions of DDR components under stress conditions [16–18].

TopBP1, as a scaffold protein, is indispensable for ATR activation. It not only interacts with ATR via its BRCT domains but also undergoes dynamic regulation through PTMs. For instance, studies have shown that TopBP1 is ubiquitinated by the E3 ubiquitin ligase hHYD and deubiquitinated by USP13, while its phosphorylation enhances its recruitment to DNA damage sites [18, 19]. Despite these insights, the precise regulatory mechanisms underlying TopBP1's role in replication stress and the functional relevance of its ubiquitination remain incompletely characterized [18, 19].

Emerging evidence implicates PHD and Ring Finger Domains 1 (PHRF1) as a critical regulator of genome stability. PHRF1, an E3 ubiquitin ligase, has been identified as a tumor suppressor that modulates various cellular processes, including TGF-β signaling, cytoplasmic relocation of the promyelocytic leukemia protein, and the repair of DNA double-strand breaks through non-homologous end joining [20–23]. While PHRF1's involvement in these pathways highlights its role in maintaining genomic integrity, its function in the replication stress response remains largely unexplored.

In the current study, we elucidate a novel role of PHRF1 in replication-related DDRs. We demonstrate that PHRF1 localizes to stalled replication forks, interacts with TopBP1, and promotes TopBP1 mono-ubiquitination, thereby enhancing TopBP1-dependent ATR activation. Furthermore, PHRF1 deficiency causes compromised ATR axis signaling, delayed restart of stalled replication fork in response to replication stresses, and sensitizes cells to replication stress-inducing agents. Moreover, *Phrf1* knockout mice exhibit increased genomic instability, while low PHRF1 expression correlates with chromosomal instability (CIN) in human cancers. Overall, our findings established PHRF1 as a key regulator of replication stress response by facilitating TopBP1-mediated ATR activation.

Materials and methods

Cell culture

HEK293T (CRL-3216), HCT116 (CCL-247), and U2OS (HTB-96) cell lines were purchased from ATCC and were cultured in Dulbecco's modified Eagle's medium or McCoy's 5A medium supplemented with 10% fetal bovine serum at 37°C in 5% (v/v) CO_2.

Plasmids and antibodies

pcDNA3-LacR-TopBP1 (#31317) vector was purchased from Addgene. Constructs of SFP-TopBP1 (WT, ΔBRCT1, ΔBRCT2, ΔBRCT3, ΔBRCT4, ΔBRCT5, ΔBRCT6, ΔBRCT7, and ΔBRCT8) were gifts from Dr Junjie Chen and were sub-cloned into pLVX3, pLVX6 vectors. Flag-PHRF1 vector was a gift from Dr Junjie Chen. PHRF1 was sub-cloned into pLVX3 vector. All truncated or site mutants of TopBP1 or PHRF1 were generated by site-directed mutagenesis (Agilent).

Anti-PHRF1-N antibody was generated by Cocalico Biologicals. The following antibodies were used: anti-PHRF1 (Abcam: ab85974, 1:2000), anti-γH2AX (Millipore: 2884537, 1:1000, Bethyl Laboratories: A300-081A, 1:1000), anti-H3 (Proteintech: 17168–1-AP, 1:5000), anti-H3K9me3 (Millipore: 07–442, 1:1000, Thermo Fisher: MA5-42567, 1:2000), anti-H3K36me3 (Cell signaling: 4909, 1:1000), anti-Phospho-ATM/ATR Substrate Motif [(pS/pT)QG] (Cell signaling: 6966S, 1:2000), anti-Rad17 (Santa Cruz: sc-17761, 1:1000), anti-Rad9 (Santa Cruz: sc-8324, 1:1000) anti-TopBP1 (Bethyl Laboratories: A300-111A, 1:1000), anti-Flag (Sigma: F1804, 1:2000, F7425, 1:2000), anti-His (Santa Cruz: sc-8036,1:2000), anti-phospho ATR (T1989) (Genetex: GTX128145, 1:1000), anti-ATR (Cell signaling : 13934, 1:1000), anti-phospho Chk1 (S345) (Cell signaling : 2348, 1:1000), anti-Chk1 (Santa Cruz: sc-8408, 1:2000), anti-phospho RPA32 (S33) (Bethyl Laboratories: A300-246A-M, 1:2000), anti-RPA32 (Santa Cruz: sc-56770, 1:2000), anti-Ub (Santa Cruz: sc:8017, 1:2000), anti-α-tubulin (Sigma: T6557, 1:5000), anti-GAPDH (Proteintech: 60004–1-Ig, 1:2000), anti-β-actin (Sigma: A2228, 1:2000), anti-GFP (Santa Cruz: sc-9996, 1:1000), anti-HA (Sigma: H6908, 1:2000), anti-S-tag (Abcam: ab78281, 1:2000), anti-BrdU (BD Bioscience: 347580, 1:200, Abcam: ab6326, 1:2000), anti-CD71 (eBioscience: 11-0711-82, 1:100).

shRNAs, sgRNAs, and siRNA

Nontarget control shRNA and PHRF1 shRNAs were purchased from Sigma. PHRF1 shRNA #1: TTGATAGTTCTTCGGTCATAG, PHRF1 shRNA #2: GACATGAAGTTTGAGTATTTG. PHRF1 knockout HCT116 and U2OS cells were generated using CRISPR/Cas9 with two sgRNAs: sgRNA #1: TCCGAGGATTCTGAAGACGA and sgRNA #2: GCATTCAGAGACCAGGCCGTGGG (Thermo Fisher). TopBP1 siRNA was purchased from Thermo Fisher (Cat: 4392420).

DNA transfections were performed using TransIT-X2 (MIRUS Bio). Lentiviruses for infection of HCT116 and U2OS cells were packaged in HEK293T cells. Medium containing lentivirus was collected 48 h after transfection. This harvested medium was then added to the target cells for subsequent experiments, with 8 μg/ml polybrene included to enhance infection efficiency.

Chromatin instability signature

PHRF1 expression (as log-RPKM) and somatic mutation calls by MuSE, MuTect2, SomaticSniper, and VarScan2 in breast cancer were downloaded from UCSC XenaBrowser (https://xenabrowser.net) GDC-TCGA-BRCA cohort. High

confident mutation counts were calculated from consistent calls between at least two callers. Homologous recombination deficiency (HRD) scores and HRD subcomponent scores (LST: large scale transition, TAI: telomeric allelic imbalances, and LOH: loss of heterozygosity) [24], and weighted genomic integrity index (wGII) [25] were downloaded from previous publications. Samples were categorized by PHRF1 expression using upper 33% and lower 33% as cutoffs based on sample availability for each score. Statistical significance was tested using the Mann–Whitney–Wilcoxon test.

Comet assay

The Comet Assay Single-Cell Gel Electrophoresis Assay Kit (Trevigen) was used according to the manufacturer's protocol. Briefly, cells were collected and rinsed twice with ice-cold phosphate buffered saline (PBS); 1×10^5 cells/ml were mixed with 1% low melting agarose at 37°C at the ratio of 1:10 (v/v) and immediately pipetted onto slides. The slides were immersed in the lysis buffer overnight at 4°C. Then, the slides were subjected to electrophoresis at 21 V for 45 min and stained with propidium iodide (PI) for 20 min. Images were taken using a fluorescence microscope and analyzed using ImageJ.

Immunofluorescence

U2OS cells were seeded on coverslips 24 h prior to the experiment. After treatment, the cells were fixed with a methanol:acetone mixture (1:1) at −20°C for 20 min. Following fixation, the cells were washed twice with PBS. To block nonspecific binding, cells were incubated with 5% goat serum for 30 min at RT (room temperature). Primary antibodies, diluted in PBS containing 1% bovine serum albumin (BSA), were applied to the cells and incubated for 1 h at RT. After washing with PBS, secondary antibodies, also diluted in PBS containing 1% BSA, were added and incubated for 1 h at RT. Cells were subsequently washed three times with PBS. For nuclear counterstaining, cells were incubated with DAPI for 5 min at RT, followed by two additional washes with PBS. Finally, cells were mounted with an anti-fade mounting solution and visualized using an ImageXpress pico or Micro confocal microscope (Molecular Devices).

Laser micro-irradiation

For laser micro-irradiation, U2OS cells were incubated in glass-bottom dishes (MatTek Corporation). Laser micro-irradiation was performed using a Micropoint Laser Illumination and Ablation system (ANDOR). After 10 min, cells were fixed and stained with the indicated antibodies.

Cell cycle analysis

WT (wild-type) or PHRF1 knockout cells were treated with 2 mM hydroxyurea (HU) for 24 h. After incubation, cells were washed and replaced with fresh media. Cells were harvested at the indicated time points, fixed in 70% ice-cold ethanol, and stained with PI/RNase solution (Thermo Fisher). Cell cycle distribution was analyzed on an Attune Nxt Flow cytometry (Thermo Fisher), and the data were processed using FlowJo software.

isolation of proteins on nascent DNA

iPOND (isolation of proteins on nascent DNA) assay was performed according to a published protocol [26]. Briefly, cells were labeled with 10 μM EdU for 20 min, followed by washing with washing buffer (0.5% bovine serum albumin in PBS). After washing, cells were incubated in medium containing HU for 2 h. Cells were then harvested, permeabilized with 0.25% Triton X-100 in PBS for 30 min, and incubated with click reaction buffer (1 mM biotin-azide, 100 mM $CuSO_4$, 20 mg/ml sodium L-ascorbate in PBS). After the click reaction, cells were sonicated with lysis buffer (1% SDS in 50 mM Tris–HCl, pH 8.0) and centrifuged at 14 000 rpm for 10 min. Biotin-labeled lysates were incubated overnight at 4°C with streptavidin beads. After incubation, the beads were rinsed with cold lysis buffer, followed by a wash with 1 M NaCl, and then a final wash with cold lysis buffer, with each wash lasting 5 min. Beads were then heated at 95°C in 2× Laemmli buffer for 30 min, loaded onto sodium dodecyl sulphate–polyacrylamide gel electrophoresis (SDS–PAGE), and immunoblotted with the indicated antibodies.

Immunoprecipitation and immunoblotting

For immunoprecipitation, cells were lysed with NETN buffer (20 mM Tris–HCl, pH 8.0, 100 mM NaCl, 1 mM EDTA, and 0.5% NP-40) for 10 min on ice. Whole cell lysates were centrifuged at 12 000 rpm for 10 min. Cell lysates were incubated with either an antibody and protein A beads (Amersham Biosciences) or Flag-, HA-, and S-beads at 4°C for 2 h or overnight. After incubation, beads were washed three times with NETN buffer. The bound proteins were eluted with 2× Laemmli buffer. For immunoblotting, cells were lysed in NETN buffer for 10 min on ice, followed by centrifugation at 12 000 rpm for 10 min. Supernatants were heated at 95°C for 10 min in 2× Laemmli buffer. Cells were lysis by sonication and then centrifuged at 12 000 rpm for 10 min. After centrifugation, the supernatants were heated at 95°C for 10 mins in 2× Laemmli buffer, loaded to SDS–PAGE, and immunoblotting with the indicated antibodies.

Denaturing his pull-down

Transiently transfected or virus-infected cells were harvested and washed once with PBS. The cells were then lysed in a denaturing urea lysis buffer containing 8 M urea, 0.1 M NaH_2PO_4, 30 mM NaCl, and 10 mM Tris (pH 8.0). The lysates were sonicated and incubated with Ni-NTA agarose beads (QIAGEN) for 1–2 h at RT to allow binding of the target protein to the beads. After incubation, the beads were washed three times with urea washing buffer (8 M urea, 0.1 M NaH_2PO_4, 300 mM NaCl, and 10 mM Tris, pH 8.0) to remove nonspecifically bound proteins. The input samples and bead-bound proteins were then boiled in Laemmli sample buffer, separated by SDS–PAGE, and analyzed by immunoblotting.

Proximity ligation assay

Cells were washed in ice-cold PBS and fixed with methanol:acetone (1:1) at −20°C for 20 min. Proximity ligation assay (PLA) was then performed using a Duo-link *in situ* PLA kit (Sigma) according to the manufacturer's instructions. Briefly, samples were blocked in blocking solution at 37°C for 1 h and then incubated with a mixture of primary antibodies (1:1000) at 4°C overnight. Then, the cells

were incubated with probes at 37°C for 1 h, followed by hybridization, ligation, amplification, and detection. Nuclei were stained with DAPI. The coverslips were mounted onto glass slides with the anti-fade solution and visualized using an ImageXpress Micro confocal microscope (Molecular Devices).

DNA fiber assay

To assess the restart efficiency of stalled replication forks, cells were labeled with 25 μM IdU for 20 min and then washed twice with medium. The cells were then treated with 4 mM HU for 2 h. After a subsequent washing with medium, cells were recovered in fresh medium with 200 μM CldU for the indicated duration. Cells were then trypsinized, resuspended in PBS to a density of 2.5×10^5 cells/ml and diluted 1:40 with unlabeled cells at the same density. A 5 μl aliquot of cells was mixed with 15 μl of lysis buffer (200 mM Tris–HCl, pH 7.4, 50 mM EDTA, and 0.5% SDS) on a clean glass slide. After 8 min of incubation, the slides were tilted at 15° to horizontal, allowing the lysate to slowly flow down along the slide. The slides were then air-dried, fixed in 3:1 methanol/acetic acid, and stored at 4°C overnight. The slides were treated with 2.5 M HCl for 1 h, neutralized in 0.1 M $Na_2B_4O_7$, pH 8.5, and rinsed three times in PBST (PBS with 0.1% Tween-20). The slides were then blocked in blocking buffer (PBST containing 1% BSA) for 20 min and incubated with anti-BrdU antibodies (BD Bioscience: 347580, Abcam: ab6326) in blocking buffer at 37°C for 1 h. After washing, secondary antibodies were diluted in PBS containing 1% BSA and incubated with the cell at RT for 1 h. After incubation, the slides were washed once with low-salt TBST (36 mM Tris–HCl pH 8.0, 50 mM NaCl, 0.5% Tween-20) and three times with PBST. After washing, cells were mounted with anti-fade solution and visualized using a Nikon eclipse 80i fluorescence microscope. All fiber lengths were measured using ImageJ.

Flow cytometry analysis

For cell cycle or sub-G1 analysis, WT cells or PHRF1 knockout cells were treated with 2 mM HU. After 24 h, cells were washed, replaced with fresh medium, and harvested by trypsinization at the indicated time points. Cells were fixed in 70% ice-cold ethanol, stained with PI/RNase solution (Thermo Fisher), and analyzed using an Attune Nxt Flow cytometer (Thermo Fisher). For immunostaining, WT cells or PHRF1 knockout cells were fixed with 70% ice-cold ethanol and then permeabilized with 0.25% Triton X-100 in PBS. Cells were incubated with the indicated primary antibodies for 3 h at RT, followed by incubation with the appropriate secondary antibodies for 1 h at RT. Cells were treated with PI/RNase solution (Thermo Fisher) and analyzed on an Attune Nxt Flow cytometer (Thermo Fisher), and data were analyzed using Flow Jo.

Colony formation assay

Five hundred to one thousand cells were plated in triplicate in each well of six-well plates. Sixteen hour later, cells were treated with camptothecin (CPT), HU, ultraviolet (UV), or fluorouracil (5-FU), and cultured for 10–14 days at 37°C to allow colony formation. Colonies were stained with Giemsa and counted. Results were normalized to plating efficiencies.

Generation of *Phrf1*$^{-/-}$ Mouse

Phrf1 knockout mice were generated by Casgene Biotech Co., Ltd. Zygotes were collected from mating superovulated C57BL/6 females with males and were injected with a mixture of Cas9 mRNA (80 ng/ul), sgRNA (40 ng/ul), and donor vector (8 ng/ul). Microinjections were performed into the male pronucleus of fertilized oocytes. The injected zygotes were transferred into pseudopregnant CD1 female mice, resulting in the birth of viable adult mice were obtained. The correctly targeted mice were determined by polymerase chain reaction (PCR) or sequencing. Primer sequences used for genotyping wereas follows: primer-F: GGTTTAGTCATTAGCACCATCTTCTCTGA; primer-R: CGTTGCCATTTCTACTCCATCTTCTG. Two loxP elements flanking exon 4 were introduced into a murine *Phrf1* gene using the CRISPR/Cas9 method. Homozygous floxed male and female mice (*Phrf1*$^{fl/fl}$) were then crossed with B6.129-Gt (ROSA)26Sor$^{tm1\ (cre/ERT2)Tyj/J}$ transgenic mice to generate *Phrf1*$^{-/-}$ mice. In the current study, 6–10-week-old mice of both sexes were used. All animal procedures were approved by the Mayo Clinic Institutional Animal Care and Use Committee (IACUC).

Preparation of mouse splenocyte for flow cytometry and metaphase spread

Spleens were harvested from mice aged 6–12 weeks and homogenized using 70 μm meshes. For quantification of genomic instability, harvested splenocytes were fixed with 70% ethanol at 4°C overnight. Fixed cells were permeabilized by 0.25% Triton X-100 in PBS at 4°C for 10 min. After permeabilization, cells were then washed with PBS and stained with γH2AX antibody (Millipore) at RT for 2 h. Following washing, cells were stained with FITC-conjugated secondary antibody (Jackson ImmunoResearch) at RT for 1 h. After staining, cells were washed and incubated with PI/RNase solution (Thermo Fisher) at RT for 30 min. The samples were analyzed using an Nxt Attune flow cytometry (Thermo Fisher), and data were analyzed using FlowJo. For metaphase spread, harvested splenocytes were incubated with concanavalin A (2.5 μg/ml) for 72 h and then treated with colcemid (Gibco). After incubation, cells were swollen by incubating in prewarmed 75 mM KCl at 37°C for 20 min. Following centrifugation, cells were fixed with Carnoy's buffer (3:1 methanol:acetic acid) at RT for 10 min. The cells were spun down for 4 min at 1000 rpm, and the supernatant was aspirated. The cells were resuspended with Carnoy's buffer twice before being dropped on the slide and allowed to air dry for at least 10 min. Finally, the slides were stained with Giemsa solution (Sigma).

Micronucleus assay

The micronucleus assay was performed using mice aged 6–12 weeks. Mouse blood was collected and mixed with 100 μl of PBS supplemented with 1000 U/ml of heparin (Calbiochem). The blood suspension was then added to 1 ml of methanol and stored at −80°C overnight. Fixed blood cells were washed with bicarbonate buffer (0.9% NaCl, 5.3 mM $NaHCO_3$). The cells were then suspended in 100 μl of bicarbonate buffer and incubated with 1 μl of FITC-conjugated CD71 antibody (Gentex) at 4°C for 45 min. After incubation, the cells were washed with bicarbonate buffer and resuspended in PI/RNase solution (Thermo Fisher) at RT for 30 min. The samples were an-

alyzed using an Attune Nxt Flow Cytometer (Thermo Fisher), and data were analyzed with FlowJo software.

Statistics and reproducibility

Data in bar and line graphs are presented as mean ± standard error of mean of at least three independent experiments. All western blot assays shown were successfully repeated at least three times.

Results

PHRF1 expression correlates with genomic stability

PHRF1, a ring finger family protein, has been linked to systemic lupus erythematosus [27]. However, the role in cancer biology remains poorly understood. To investigate its potential involvement in genomic stability, we examined the relationship between PHRF1 expression and various genomic integrity markers in breast cancer patient samples from The Cancer Genome Atlas (TCGA). Samples were categorized based on PHRF1 expression, using the upper and lower 33% as cutoffs for high and low expression groups, respectively, based on available data for each score. Our analysis revealed a significant inverse correlation between PHRF1 expression and genomic instability. Specifically, patients with low PHRF1 expression exhibited higher levels of genomic instability, as indicated by increased wGII, HRD score, LST, TAI, and LOH (Fig. 1A–E). Additionally, low PHRF1 expression was associated with a higher number of somatic mutations per genome (Nmut) (Fig. 1F). These findings suggest that lower PHRF1 expression correlates with increased CIN and mutation burden in cancer patients, supporting the hypothesis that PHRF1 may play a role in maintaining genomic stability.

To test this hypothesis, we knocked out PHRF1 in HCT116 cells and observed that depletion of PHRF1 increased CIN incidents such as SCE, Holliday junctions, and chromosome break. (Fig. 1G–J and Supplementary Fig. S1A). Further investigation into spontaneous DNA damage using comet assays and multinucleated cell analysis revealed that PHRF1 knockout cells accumulated DNA damage (Fig. 1K–O). The flow cytometry analysis showed a dramatic increase in γH2AX (a DNA damage marker) fluorescence intensity in PHRF1 knockout cells compared to WT cells (Fig. 1P and Q). These results provide strong evidence that PHRF1 is involved in maintaining genomic stability.

PHRF1 is recruited to replication forks

To elucidate the role of PHRF1 in DDR, we first examined its cellular localization following DNA damage. PHRF1 was recruited to DNA damage sites induced by laser microirradiation or HU treatment, indicating its involvement in DDR (Fig. 2A–C). Additionally, we observed that unstressed PHRF1 knockout cells exhibited increased S-phase population compared to WT cells (Fig. 2D and E), implying a potential role for PHRF1 in DNA replication-associated DDR mechanisms.

To further investigate this, we assessed the recruitment of PHRF1 to stalled replication forks using the native iPOND assay. This technique allows for the identification of replication-associated proteins by isolating nascent DNA-binding proteins [28]. Nascent DNA at replication forks was labeled with EdU, followed by biotin conjugation to EdU via a click reaction. Subsequently, nascent DNA-binding proteins were enriched through affinity purification (Fig. 2F). As shown in Fig. 2G, PHRF1 localizes to replication forks. This localization was enhanced upon HU treatment, reinforcing the hypothesis that PHRF1 is involved in the replication-related DDR (Fig. 2H).

Next, we sought to understand how PHRF1 is recruited at stalled replication forks. Previous studies showed that the PHD finger domain acts as a reader for histone modifications (e.g. H3K9me3, H3K4me3, and H3K4me0) [29]. In addition, it has been reported that histone H3 methylation, like H3K9me3, is elevated at stalled replication forks [30]. Based on this, we hypothesized that PHRF1 might be recruited at the DNA damage sites by interacting with modified histone marks through its PHD domain. To test this, we first examined whether H3K9me3 is involved in DDR. As shown in Supplementary Fig. S1B, H3K9me3 accumulated and colocalized with γH2AX upon micro-irradiation, in line with previous findings [31]. Given this observation, we investigated the role of histone modifications in PHRF1 recruitments under replication stress. Strikingly, chaetocin (an inhibitor of H3K9 methylation transferase SUV39H1) treatment completely abolished PHRF1 recruitment to stalled replication forks as well as micro-irradiation or HU induced DNA damage sites and inhibited ATR activation (Fig. 2H, I and Supplementary Fig. S1C–E).

To further confirm that PHRF1 directly binds to methylated histone, we performed an *in vitro* pull-down assay using biotin-labeled histone peptides. PHRF1 showed a strong binding affinity for H3K9me3 and H3K36me3, but a weaker interaction with H3K27me3, and no binding to unmodified H3 or H4 peptides (Fig. 2J and Supplementary Fig. S1F–H). This interaction was also confirmed by coimmunoprecipitation (coIP) of PHRF1 with histones containing H3K9me3, which was further enhanced upon HU treatment (Fig. 2K). To determine the specific histone modification critical for PHRF1 recruitment, we analyzed histone modifications in chromatin fractions. The immunoprecipitation assays using chromatin fraction revealed that PHRF1 interacts with H3K9me3 and chaetocin treatment reduced this interaction (Fig. 2K). Moreover, the PHD domain of PHRF1 was crucial for its interaction with H3K9me3, as a PHRF1 mutant lacking the PHD domain showed no binding to either H3K9me3 peptides or chromatin (Fig. 2J–L). Although PHRF1 also binds to H3K36me3, we evaluated the H3K36me3 levels at the replication fork with or without chaetocin treatment. As shown in Fig. 2H, both PHRF1 and H3K9me3 decreased at the replication fork under chaetocin treatment, whereas H3K36me3 levels remain unchanged. Furthermore, total H3K36me3 is unaffected by 24 h chaetocin treatment (Supplementary Fig. S1E). These findings indicate that PHRF1 interacts with H3K9me3 via its PHD domain, and this interaction is crucial for the recruitment of PHRF1 to stalled replication forks.

We next investigated whether PHRF1 undergoes PTMs in response to replication stress. As shown in Fig. 2M and N, upon HU treatment, PHRF1 was phosphorylated at consensus ATM/ATR phosphorylation motifs (S/TQ sites). This was further diminished by pretreatment with VE-822, a selective ATR inhibitor, indicating that PHRF1 is a potential phosphorylation target of ATR. To identify potential ATR phosphorylation sites on PHRF1, we consulted a public database (www.phosphosite.org) and found two potential serine residues (S925 and S1389). Specifically, mutation of S925 to alanine

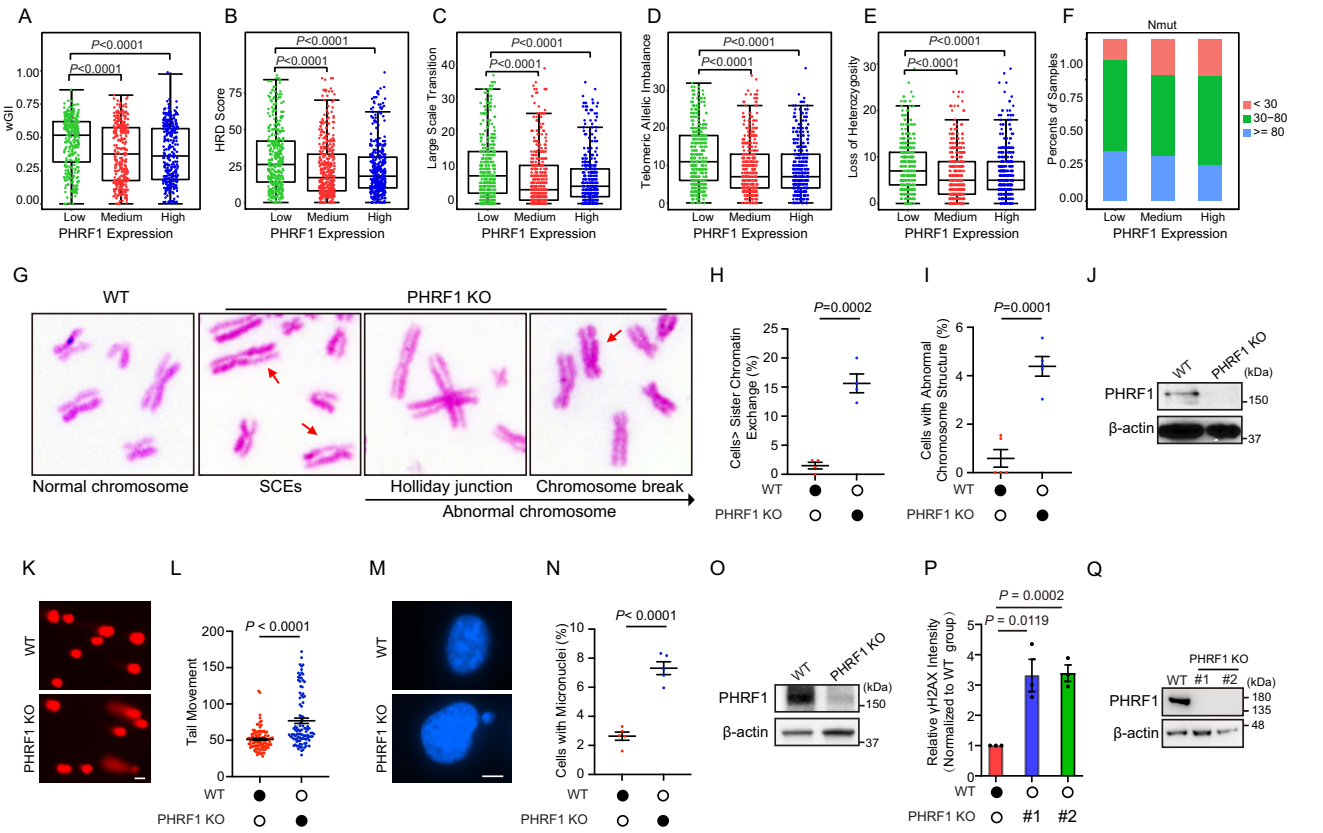

Figure 1. PHRF1 expression highly correlates with genomic stability. TCGA Breast Cancer database was analyzed to evaluate genomic instability. The analysis examined the association of PHRF1 expression levels with chromosomal instability characteristics, including wGII (**A**), HRD score (**B**), LST (**C**), TAI (**D**), LOH (**E**), and the Total Number of Somatic Exome Mutations per genome (Nmut) (**F**). Samples were categorized by PHRF1 expression using upper 33% and lower 33% as cutoffs based on sample availability for each score. Statistical significance was tested using the Mann–Whitney–Wilcoxon test. (**G–I**) Metaphase spreads were generated in PHRF1 knockout and WT HCT116 cells. Sister chromatin exchanges (SCEs) and abnormal chromosomes were determined. The graphs in panels (H, I) represent mean ± standard error of mean, two-tailed, unpaired *t*-test; $n \geq 3$ independent experiments. (**J**) PHRF1 knockout efficiency in panels (G–I) was evaluated using western blotting (WB). (**K**) Spontaneous DNA damage accumulation was measured in PHRF1 knockout or WT HCT116 cells using a comet assay. (**L**) The comet tail movement was measured from 100 cells in each group. The graph represents mean ± standard error of mean, two-tailed, unpaired *t*-test. (**M**) PHRF1 knockout or WT HCT116 cells were stained with DAPI to detect micronuclei. Scale bars, 10 μm. (**N**) Quantification of the percentage of cells with micronuclei. The graph represents mean ± standard error of mean, two-tailed, unpaired *t*-test. $n \geq 3$ independent experiments. (**O**) PHRF1 knockout efficiency in panels (K–N) was evaluated using WB. (**P**) PHRF1 knockout or WT HCT116 cells were stained with an anti-γH2AX antibody to detect spontaneous DNA damage accumulation in chromatins. γH2AX intensity was quantified by flow cytometry and normalized to the WT cells group. The graph represents mean ± standard error of mean, two-tailed, unpaired *t*-test. $n = 3$ independent experiments. (**Q**) PHRF1 knockout efficiency in panel (P) was evaluated using WB.

(S925A) diminished phosphorylation of PHRF1 upon HU treatment (Fig. 2O), while mutation of S1389 had no effect. Consistently, S925A mutation significantly reduced PHRF1 localization at stalled replication forks and damaged chromatin (Fig. 2P), highlighting the importance of S925 phosphorylation for PHRF1 recruitment to replication forks in response to HU-induced replication stress. In conclusion, our data suggest that PHRF1 is recruited to the replication fork in a histone methylation and S925 phosphorylation-dependent manner.

The regulation of replication stress responses by PHRF1 is TopBP1-dependent

To identify potential partners of PHRF1 in the regulation of stalled fork restart, we expressed FLAG-tagged PHRF1 in HEK293T cells and conducted coIP experiments. Our results revealed a direct interaction between PHRF1 and TopBP1 (Figs 2M and 3A and Supplementary Fig. 2A). Notably, this interaction is increased following replication stress induced by HU (Fig. 3B). However, the PHRF1 S925A mutant exhibited a marked reduction in this interaction (Fig. 3B), likely due to impaired PHRF1 recruitment to chromatin.

To map the interaction between PHRF1 and TopBP1, we generated a series of truncated mutants of both proteins: PHRF1 (WT, ΔRING, and ΔPHD) and TopBP1 (WT, ΔBRCT1, ΔBRCT2, ΔBRCT3, ΔBRCT4, ΔBRCT5, ΔBRCT6, ΔBRCT7, and ΔBRCT8). Immunoprecipitation assays demonstrated that the PHD domain of PHRF1 and the fourth BRCT domain of TopBP1 were both required for their interaction (Fig. 3C, D and Supplementary Fig. S2B).

Given these findings and the involvement of PHRF1 in the DDR, we next examined its impact on ATR-Chk1 activation. As shown in Fig. 3E–G and Supplementary Fig. S2C, both PHRF1 knockdown or knockout cells exhibited reduced ATR-dependent phosphorylation of RPA32 (S33) or Chk1 (S345) following HU or CPT treatment. These results suggest that PHRF1 is important for efficient ATR signaling. Importantly, the defect in ATR activation was restored by the ectopic expression of WT PHRF1 but not the ΔRING or ΔPHD mutant,

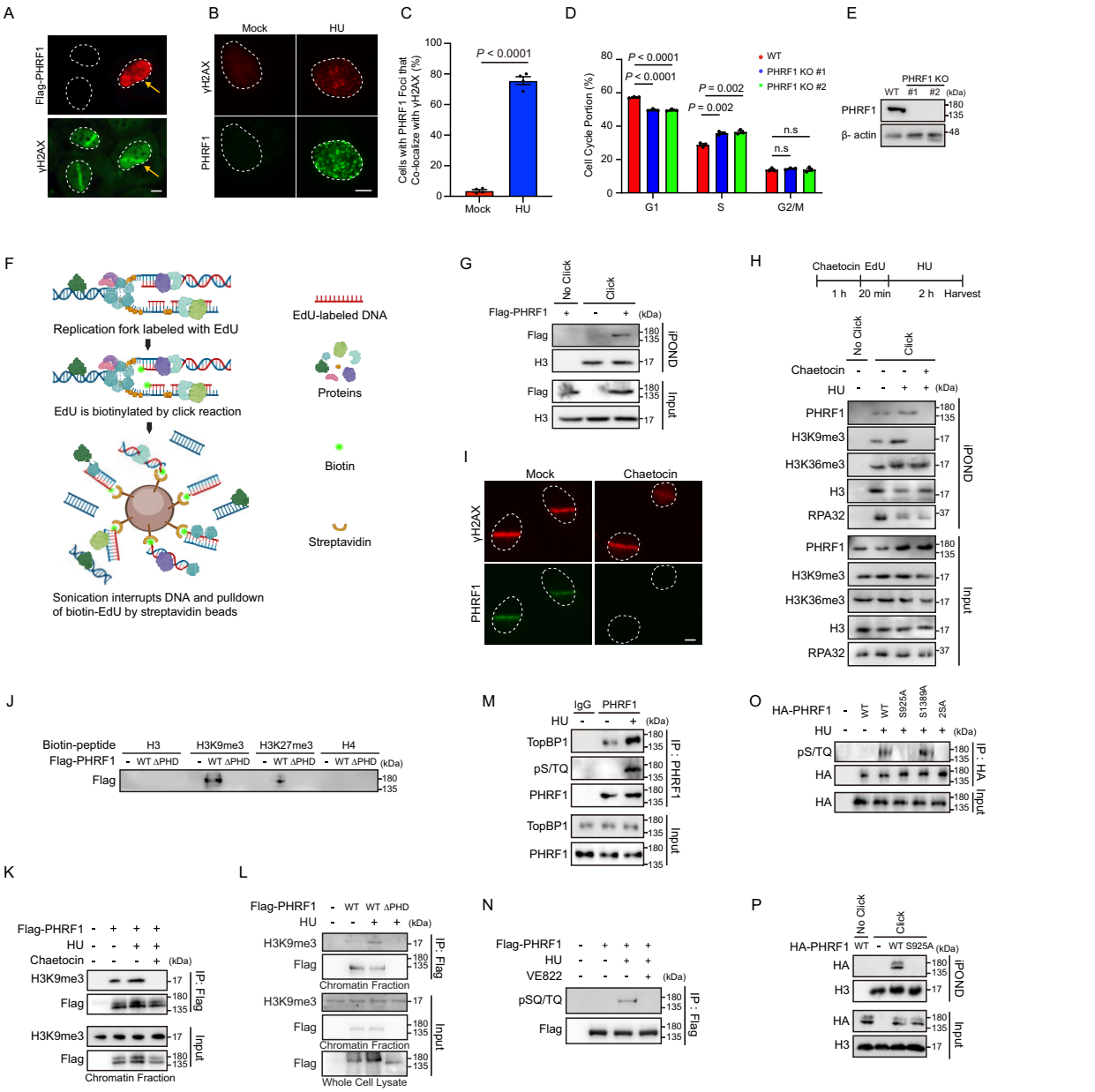

Figure 2. PHRF1 is recruited to replication forks. (**A**) Flag-PHRF1 overexpressed U2OS cells were stained with anti-Flag (PHRF1) and γH2AX antibodies 10 min post micro-irradiation. Scale bars, 10 μm. (**B**, **C**) PHRF1 and γH2AX colocalization were evaluated by immunofluorescence assay. The graphs in panels (B, C) represent mean ± standard error of mean, two-tailed, unpaired *t*-test; $n = 4$ independent experiments. Scale bars, 10 μm. (**D**, **E**) Cell cycle distribution was determined by flow cytometry in PHRF1 knockout or WT HCT116 cells. The proportions of cells in each cell cycle phase were determined using Modifit. The data in panel (D) are presented as mean ± standard error of mean, with statistical significance assessed using a two-tailed, unpaired *t*-test ($n = 3$ independent experiments). PHRF1 knockout efficiency in panel (D) was evaluated using WB (panel E). (**F**) Cartoon scheme for iPOND assay. Image created in BioRender. Chenghui, C. (2025). https://BioRender.com/r26o549. (**G**) HCT116 cells expressing Flag-PHRF1 were incubated with 10 μM EdU. Replication fork proteins were isolated by native-iPOND. (**H**) HCT116 cells were preincubated with 50 nM chaetocin, followed by incubated with 10 μM EdU and 10 mM HU for the indicated durations. Replication fork proteins were then isolated by native-iPOND. (**I**) U2OS cells were pre-treated with 50 nM chaetocin for 1 h, followed by micro-irradiation. The cells were then costained with anti-PHRF1 and γH2AX antibodies 10 min after micro-irradiation. Scale bars, 10 μm. (**J**) Biotin-labeled histone peptides were incubated with the indicated 293T cell lysates, captured with streptavidin beads, and analyzed by SDS–PAGE. (**K**) 293T cells were transfected with Flag-PHRF1 constructs for 48 h, then pretreated with or without 50 nM chaetocin for 1 h, followed by treatment with 10 mM HU for 2 h. The chromatin fraction was immunoprecipitated using Flag antibody-conjugated beads, and H3K9me3 and Flag-PHRF1 were detected by immunoblotting with the indicated antibodies. (**L**) 293T cells were transfected with the indicated Flag-PHRF1 constructs for 48 h. The chromatin fraction was immunoprecipitated with Flag antibody-conjugated beads. H3K9me3 and Flag were immunoblotted with the indicated antibodies. (**M**) 293T cells were treated with or without 10 mM HU for 2 h. Whole cell lysates were immunoprecipitated with PHRF1 antibody and rabbit IgG. TopBP1, p-S/TQ, and PHRF1 were blotted with the indicated antibodies. (**N**) 293T cells were transfected with Flag-PHRF1 for 48 h, followed by pretreatment with 1 μM VE-822 for 1 h. After VE-822 treatment, cells were incubated with 10 mM HU for 1 h. Whole cell lysates were immunoprecipitated using Flag antibody-conjugated beads. Flag and p-S/TQ were blotted with the indicated antibodies. (**O**) 293T cells were transfected with HA-PHRF1 WT, S925A, S1389A, or 2SA (S925A/S1389A) for 48 h, followed by treatment with 10 mM HU for 1 h. Whole cell lysates were immunoprecipitated using HA antibody-conjugated beads. HA and p-S/TQ were blotted with the indicated antibodies. (**P**) HCT116 cells were transfected with HA-PHRF1 or HA-PHRF1 S925A for 48 h and then incubated with 10 μM EdU and 10 mM HU for 2 h. Replication fork proteins were isolated by native-iPOND. HA and H3 were immunoblotted with the indicated antibodies.

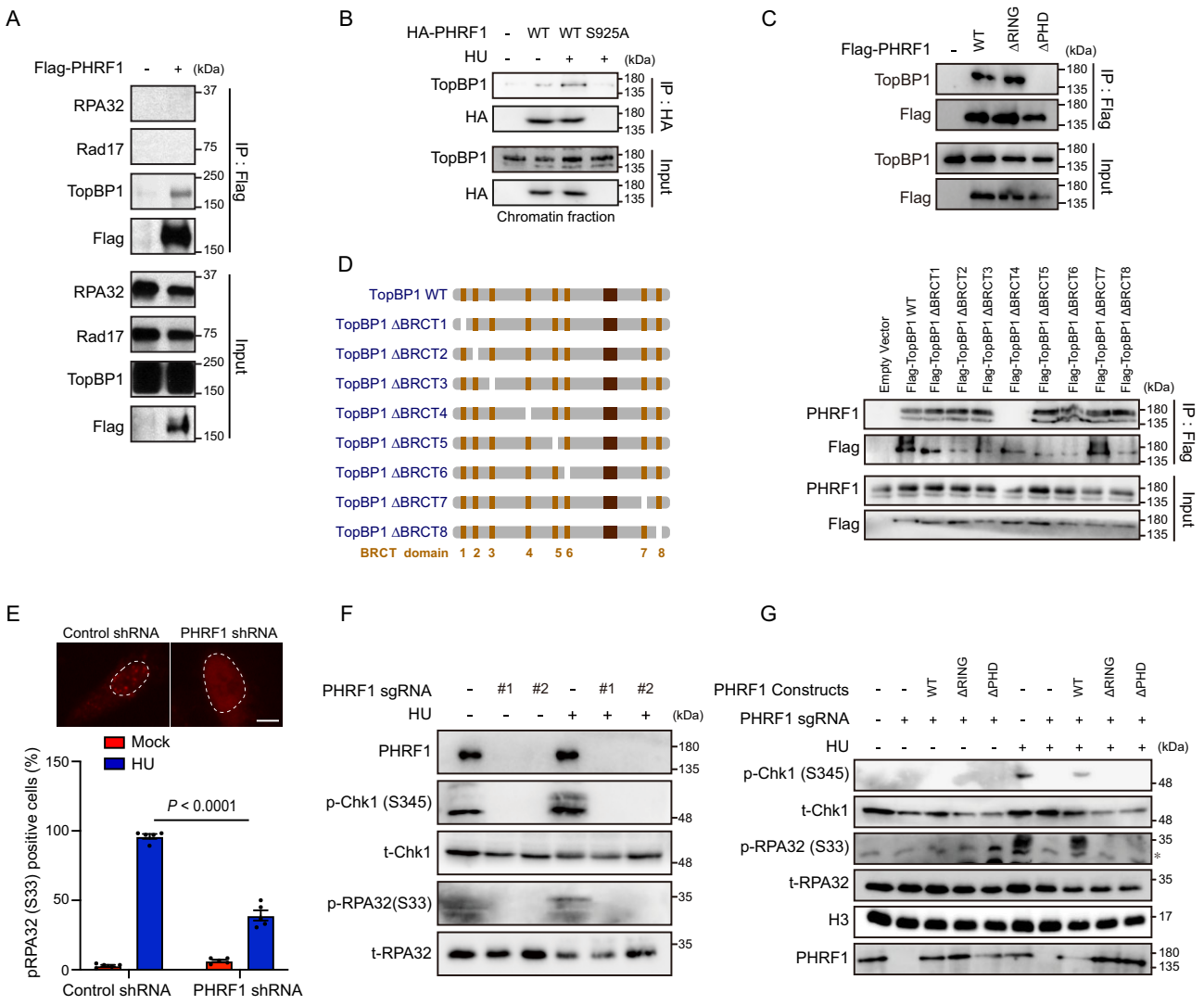

Figure 3. PHRF1 is important for ATR-Chk1 activation. (**A**) 293T cells were transfected with Flag-PHRF1 for 48 h. Whole cell lysate was immunoprecipitated with Flag antibody-conjugated beads and blotted with the indicated antibodies. (**B**) 293T cells were transfected with HA-PHRF1 WT or S925A mutant for 48 h, followed by treatment with or without 10 mM HU for 2 h. Chromatin fraction was immunoprecipitated with HA antibody-conjugated beads and blotted with the indicated antibodies. (**C**) 293T cells were transfected with Flag-PHRF1 WT, ΔRING, or ΔPHD for 48 h. Whole cell lysate was immunoprecipitated with Flag antibody-conjugated beads and blotted with the indicated antibodies. (**D**) Schematic representation of SFP-TopBP1 WT and truncation mutants. 293T cells were transfected with SFP-TopBP1 WT or SFP-TopBP1 mutants for 48 h. Whole cell lysate was immunoprecipitated with Flag antibody-conjugated beads and blotted with the indicated antibodies. (**E**) U2OS cells were infected with lentivirus expressing control shRNA or PHRF1 shRNA. The cells were treated with or without 10 mM HU for 2 h. Phospho-RPA32 (S33) foci formation was assessed by immunofluorescence, and the percentage of phospho-RPA32 (S33) foci > 5 cells [phospho-RPA32 (S33) positive cells] was quantified and plotted. The graph represents mean ± standard error of mean, two-tailed, unpaired *t*-test; $n = 5$ independent experiments. Scale bars, 10 μm. (**F**) PHRF1 knockout and WT HCT116 cells were treated with or without 10 mM HU for 2 h, and DNA damage-related proteins were assessed by immunoblotting. (**G**) PHRF1 knockout HCT116 cells were transfected with Flag-PHRF1 WT, ΔRING, or ΔPHD for 48 h, followed by treatment with or without 10 mM HU for 2 h. The indicated DNA damage-related proteins were then assessed by immunoblotting. t-Chk1: total Chk1, t-RPA32: total RPA32. p-chk1: phosphorylated chk1 (S345), and p-RPA32: phosphorylated RPA32 (S33). *indicates nonspecific bands.

highlighting the importance of PHRF1's E3 ligase activity and chromatin recruitment for ATR activation (Fig. 3G). Taken together, these data suggest that PHRF1 is necessary to the efficient activation of ATR-Chk1 activation through its RING and PHD domains.

PHRF1 mono-ubiquitinates TopBP1

Next, we hypothesized that PHRF1 regulates TopBP1 through its E3 ligase activity. To investigate this, we first checked TopBP1 foci formation and protein level. However, no significant changes in TopBP1 foci formation and protein level were observed following PHRF1 knockout (Fig. 4A and B). Additionally, PHRF1 KO does not affect TopBP1-Rad9 interaction (Supplementary Fig. S3A).

We then assessed the ubiquitination status of TopBP1 using a denatured ubiquitination assay. After performing a His-Ub pull-down, we observed a shifted TopBP1 band (Fig. 4C). To confirm this result, we generated Flag-TopBP1-Ub-6xHis expression vectors and performed a His pull-down assay. The results demonstrated that TopBP1 could undergo mono-ubiquitination, as indicated by the size of the Ub-conjugated TopBP1 (Supplementary Fig. S3B). This mono-ubiquitination was enhanced by PHRF1 overexpression or HU treatment

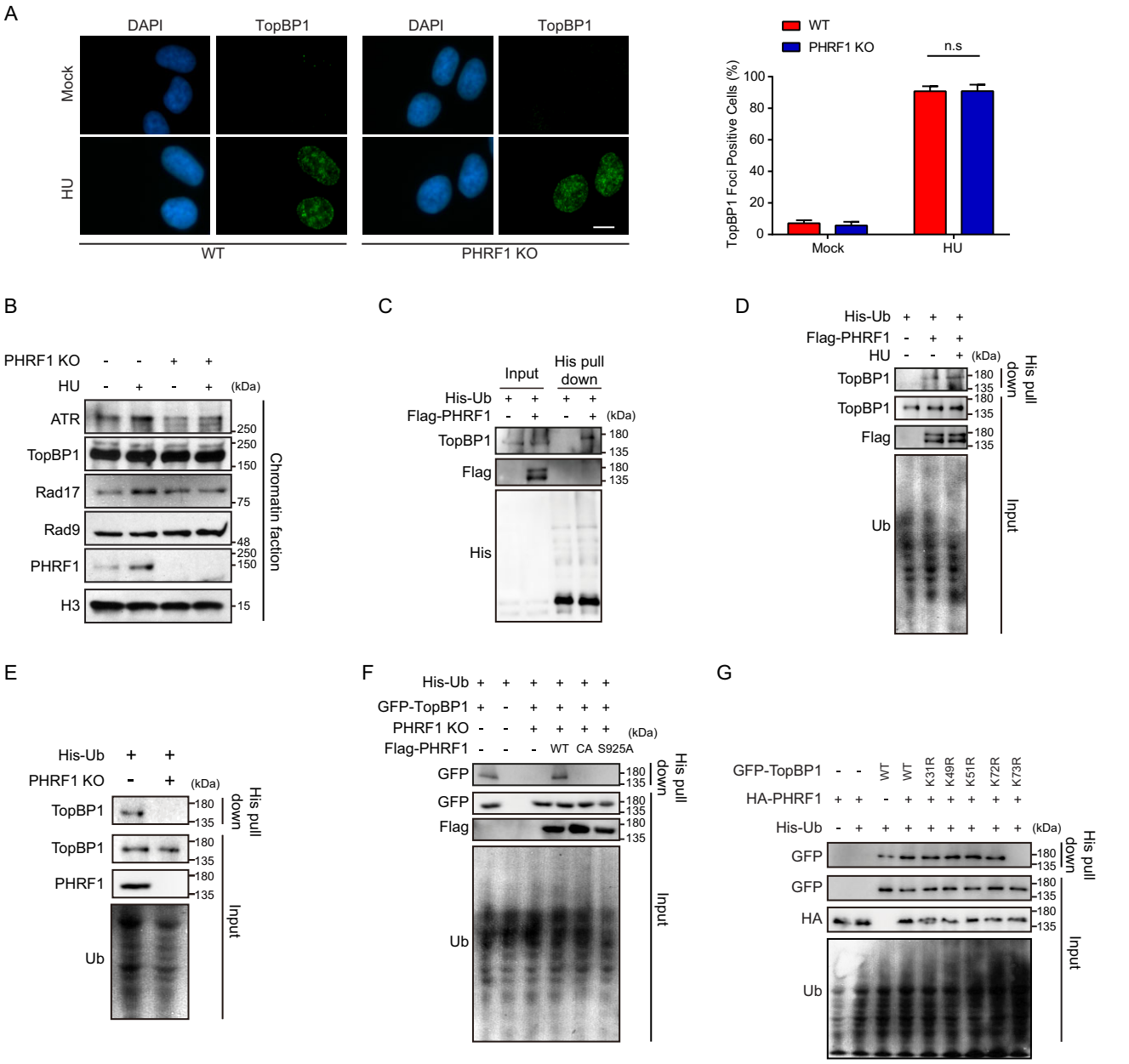

Figure 4. PHRF1 mono-ubiquitinates TopBP1 at K73. (**A**) WT or PHRF1 knockout U2OS cells were treated with or without 10 mM HU for 2 h. TopBP1 foci formation was assessed by immunofluorescence and the percentage of cells with > 5 TopBP1 foci (TopBP1 positive cells) was quantified and plotted. The graphs represent mean ± standard error of mean, two-tailed, unpaired *t*-test; $n = 3$ independent experiments. Scale bars, 10 μm. (**B**) PHRF1 knockout and WT HCT116 cells were treated with 10 mM HU for 2 h. Chromatin fraction was isolated and immunoblotted using the indicated antibodies. (**C**, **D**) HCT116 cells were transfected with His-Ub and Flag-PHRF1 vector for 48 h. The cells were then treated either with vehicle (C) or 10 mM HU for 2 h (D), followed by lysis in urea denaturation buffer. The ubiquitination of TopBP1 was assessed by His pull-down, and the samples were immunoblotted with the indicated antibodies. (**E**) PHRF1 knockout and WT HCT116 cells were transfected with His-Ub vector for 48 h, followed by a His pull-down assay. (**F**) PHRF1 knockout HCT116 cells were transfected with Flag-PHRF1 WT, CA, or S925A mutant and GFP-TopBP1 vectors for 48 h, followed by a His pull-down assay. (**G**) HCT116 cells were transfected with His-Ub, HA-PHRF1, GFP-TopBP1 WT, and different KR mutant vectors for 48 h, followed by a His pull-down assay. (E–G) The cells were lysed using a urea denaturation buffer. The ubiquitination of TopBP1 was assessed by His pull-down, and the samples were immunoblotted with the indicated antibodies.

(Fig. 4D) and reduced upon PHRF1 knockout (Fig. 4E). To further validate this finding, we conducted a reconstitution assay using WT PHRF1, a catalytically inactive C108A mutant, and an S925A mutant in PHRF1 knockout cells. Only WT PHRF1 restored TopBP1 ubiquitination, whereas neither the C108A nor S925A mutant was able to do so (Fig. 4F). These results indicate that both the E3 ligase activity and phosphorylation of PHRF1 are essential for TopBP1 ubiquitination.

We next sought to identify the specific ubiquitination site on TopBP1. Through a screen of potential ubiquitination sites, we identified Lysine 73 (K73) as the primary site of mono-ubiquitination by PHRF1 (Fig. 4G). Overall, our data supports that TopBP1 is mono-ubiquitinated by PHRF1 at K73.

PHRF1 promotes the interaction between TopBP1 and ATR

Our results suggest that PHRF1 mediates the mono-ubiquitination of TopBP1 without affecting its stability or foci formation under replication stress (Fig. 4A and B). Previous studies have shown that the interaction between TopBP1 and ATR increases under replication stress [12–14]. We hypothesize that PHRF1 regulates this interaction by mediating TopBP1 ubiquitination. A coIP assay reveals that TopBP1-ATR interaction is impaired in PHRF1 knockout cells under replication stress (Fig. 5A). Further investigation demonstrated that overexpression of WT PHRF1 enhanced the TopBP1-ATR interaction under HU treatment, while the CA mutant failed to do so in PHRF1 knockout (Fig. 5B). These results suggest that PHRF1 is required for the efficient interaction between TopBP1 and ATR.

To determine if TopBP1 ubiquitination is critical for the TopBP1-ATR interaction, we mutated K73 on TopBP1 (TopBP1 K73R). As shown in Fig. 5C, while TopBP1-ATR interaction is enhanced by HU treatment, K73R mutation reduced this interaction, supporting the idea that K73 ubiquitination promotes the TopBP1-ATR interaction. This led us to speculate that the ubiquitination of K73 might induce a conformational change in TopBP1, exposing the ATR activation domain (AAD), facilitating ATR binding.

To test this hypothesis, we first examined whether the N-terminal region of TopBP1 blocks AAD domain by interacting with its C-terminus to form a "closed" conformation. Immunoprecipitation results indicated that the N-terminal and C-terminal regions of TopBP1 interact with each other, with the C-terminal region being essential for ATR binding (Fig. 5D). Moreover, a competition assay demonstrated that the C-terminal region TopBP1 interacts with ATR, and this interaction is disrupted by the N-terminal region in a dose-dependent manner (Fig. 5E).

PLA, which is a powerful tool that allows for the detection of protein interactions with high specificity and sensitivity, further supported these findings. Under unstressed conditions, the PLA signals were strong, indicating robust interaction between the N- and C-terminal regions of TopBP1 (Fig. 5F, G and Supplementary Fig. S3C). However, HU treatment reduced PLA signals, suggesting a dissociation between the N-terminus and the C-terminus of TopBP1. Conversely, PHRF1 knockdown led to enhanced PLA signals, suggesting that PHRF1 facilitates the dissociation of the N- and C-terminal regions of TopBP1. The TopBP1 K73R mutant, which cannot be ubiquitinated by PHRF1, showed no decrease in PLA signal with HU treatment, further confirming that K73 ubiquitination regulates TopBP1 conformation (Fig. 5F and G).

These data suggest that K73 ubiquitination by PHRF1 induces a conformational change in TopBP1, exposing its ATR-activating domains and facilitating ATR interaction and activation (Fig. 5H).

PHRF1 promotes stalled replication fork restart by ubiquitinating TopBP1

The ATR-Chk1 axis signaling pathway is critical for DNA replication and recovery of stalled replication. Since our results showed that lack of PHRF1 causes defects in ATR activation and ATR-TopBP1 interaction, we investigated whether PHRF1 deficiency leads to the accumulation of DNA replication errors under replication stress. To investigate this, we performed DNA fiber assays. PHRF1 knockout cells exhibited slightly decreased replication speed in the absence of replication stress compared to WT cells (Fig. 6A). Additionally, in the absence of replication stress, PHRF1 knockout cells did not affect new origin firing and asymmetrical replication (Supplementary Fig. S4A and B). Interestingly, under replication stress, PHRF1 knockout cells exhibited a significant reduction in replication strand lengths when compared to WT cells (Fig. 6B), which can be reversed by the expression of WT PHRF1, but not the ΔRING mutant and S925A mutant (Fig. 6C).

Furthermore, we investigated whether TopBP1 ubiquitination affects replication fork restart. As shown in Fig. 6D and E, TopBP1 deficiency reduced both replication speed and stalled fork restart, and this phenotype can be rescued by ectopic expression of TopBP1 WT, but not the K73R mutant that compromised the Ub site. These findings suggest that PHRF1-mediated ATR activation via TopBP1 ubiquitination is important for stalled replication fork restart.

Given that PHRF1 is important for ATR-Chk1 activation, replication fork stability, and stalled fork restart, we hypothesized that PHRF1 knockout cells are more sensitive to replication stress-inducing agents than WT cells. To test this hypothesis, we examined γH2AX signals and cell death after HU treatment. As shown in Fig. 6F-K, PHRF1 knockout cells accumulated more cellular DNA damage (γH2AX) and had decreased viability (SubG1 population, marker as cell death) as assessed by flow cytometry. Loss of PHRF1 results in hypersensitivity to HU, CPT, UV irradiation, and 5-FU. Taken together, our results indicate that PHRF1 promotes TopBP1-mediated ATR activation and is important for genomic stability upon stalled replication stress response.

PHRF1 maintains genomic stability *in vivo*

Accumulated replication stress commonly leads to higher levels of DNA damage and genomic instability. To investigate whether PHRF1 deficiency induces genomic instability *in vivo*, we generated *Phrf1* knockout mice (*Phrf1*$^{-/-}$). We found that constitutive *Phrf1* knockout is embryonically lethal (data not shown). Therefore, we generated conditional knockout mice using an inducible Cre/loxP system. Tamoxifen was administered intraperitoneally to induce whole-body *Phrf1* knockout in 1-month-old mice (Fig. 7A). Interestingly, *Phrf1* knockout mice exhibited growth retardation, hunched back, and early death phenotype within 40 days (Fig. 7B and C).

To examine whether *Phrf1* is involved in genomic stability *in vivo*, we examined hematopoietic cells for evidence of spontaneous CIN characterized by micronuclei formation during NCEs differentiation [10]. *Phrf1*$^{-/-}$ NCEs showed significantly increased micronuclei compared to *Phrf1*$^{+/+}$ cells (Fig. 7D and E). We also examined genomic stability by analyzing the ratio of γH2AX positive population of splenocytes in mice. *Phrf1*$^{-/-}$ cells showed a higher proportion of γH2AX positive cells compared to *Phrf1*$^{+/+}$ cells (Fig. 7F and G).

Additionally, we also prepared metaphase spreads of thymocytes to assess genomic stability and found a significant increase in spontaneous chromosome instability in *Phrf1*$^{-/-}$ cells (Fig. 7H and I). As previously reported, UV exposure damages the outermost layer of the skin, triggering rapid local responses such as keratinocyte cell death, dermal inflammation and epidermal thickening. These responses are commonly

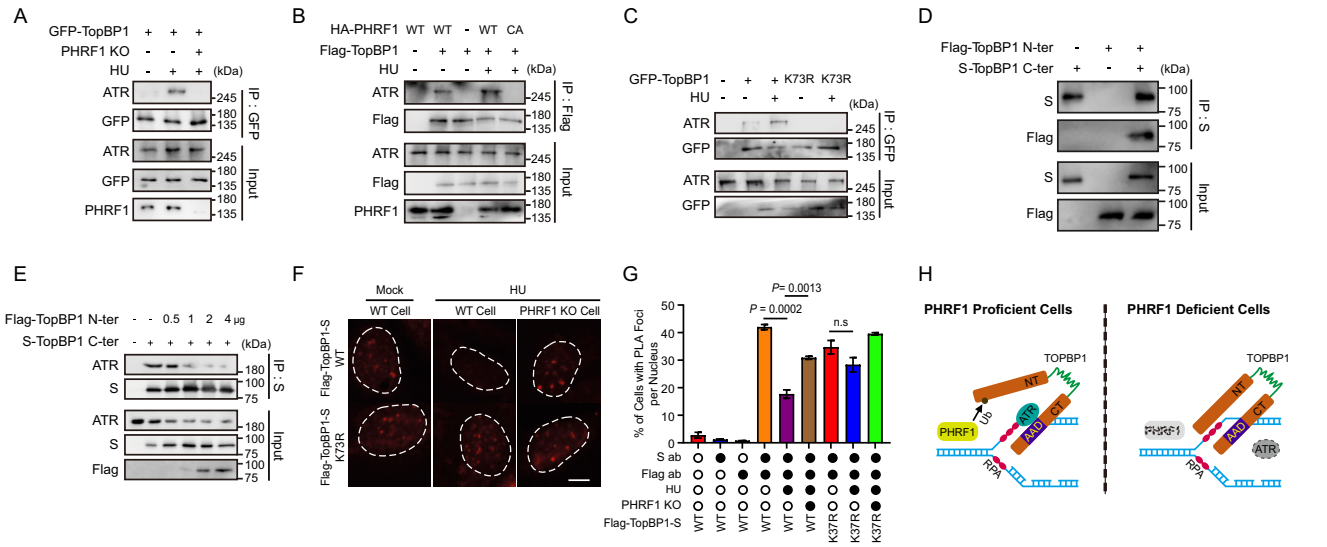

Figure 5. PHRF1 promotes the interaction between TopBP1 and ATR. (**A**–**C**) The indicated vectors were transfected into PHRF1 knockout or WT HCT116 cells. 48 h later, the cells were then treated either with vehicle or 10 mM HU for 2 h. The interaction between ATR and TopBP1 was determined by immunoprecipitation using the indicated antibodies. (**D**) HCT116 cells were transfected with S-TopBP1 C-terminus and Flag-TopBP1 N-terminus vectors for 48 h. TopBP1 N-terminus and C-terminus interaction was determined by immunoprecipitation assay using S beads. (**E**) HCT116 cells were transfected with Flag-TopBP1 N-terminus and S-TopBP1 C-terminus vectors for 48 h. The dose of N-terminus of TopBP1 vector for transfection ranges from 0.5 to 4 μg in the indicated groups, while the dose of C-terminus is 1 μg in each group. Immunoprecipitation and immunoblotting were conducted using the indicated antibodies. (**F**, **G**) PHRF1 knockout or WT U2OS cells were transfected with the indicated vectors. 48 h later, the cells were treated either with vehicle or 10 mM HU for 2 h as indicated in each group. The interaction between TopBP1 N-term and C-term was assessed by PLA. PLA foci are shown in panel (F), and the percentage PLA signal positive cells (≥ 1 PLA foci) were quantified in the graph in panel (G). Eight hundred cells were quantified for each independent experiment, $n = 3$ independent experiments. The graph represents mean ± standard error of mean, two-tailed, unpaired *t*-test. Scale bars, 10 μm. (**H**) The graphic summary of TopBP1 regulation by PHRF1.

associated with DDR and the activation of the ATR signaling pathway [32–34]. Next, we examined ATR pathway signaling following UV irradiation in Phrf1 knockout mice. As shown in Fig. 7J–L, ATR signaling activation was impaired, and epidermal thickness was significantly increased in UV-irradiated *Phrf1*$^{-/-}$ mice. Overall, our results suggest that *Phrf1* plays a crucial role in maintaining genomic stability *in vivo*.

Discussion

Accurate DNA replication is essential for the longevity of life and the transmission of genomic information to the next generation. However, DNA replication errors can lead to genomic instability, closely associated with tumorigenesis. The maintenance of replication fork stability is a critical aspect of ensuring genomic stability. ATR plays an essential role in this process, and it is critical to understand how ATR is recruited and regulated at stalled replication forks or ssDNA damage sites.

In this study, we identify PHRF1 as an important factor in the restart of stalled replication forks and the maintenance of genomic stability. We found that PHRF1 is recruited to stalled replication forks in response to replication stress in histone methylation (specifically H3K9me3) and S925 phosphorylation (S925)-dependent manner. This recruitment allows PHRF1 to function as a novel E3 ligase for TopBP1, a key regulator of ATR activation. By mono-ubiquitinating TopBP1 at lysine 73, PHRF1 induces a conformational change in TopBP1 that facilitates its interaction with ATR, thereby promoting ATR activation. Our data also demonstrate that PHRF1 deficiency results in a failure to restart stalled replication forks, heightened sensitivity to replication stress-inducing agents, and an increase in spontaneous CIN. Additionally, the conditional knockout of *Phrf1* in mice resulted in early lethality and impaired ATR-Chk1 signaling, underscoring the critical role of PHRF1 in maintaining genomic stability *in vivo*.

While ATR activation is essential for genome stability, the mechanisms by which it is regulated at replication stress sites remain an area of intense investigation. In previous studies, it had been suggested that TopBP1 underwent several PTMs, including phosphorylation or acetylation, during DDR [17]. Moreover, the dynamic regulation of TopBP1 levels has been linked to polyubiquitination by the E3 ligase hHYD-mediated polyubiquitination and USP13-mediated deubiquitination [18, 19]. In contrast, our study identifies a novel role for PHRF1 mono-ubiquitinating TopBP1, an action that promotes its conformational shift and enhances its ability to bind ATR. This finding provides new insight into the post-translational regulation of TopBP1 and ATR signaling, positioning PHRF1 as an important player in DNA replication stress responses.

Our study also opens the door to potential therapeutic implications. Given that PHRF1 acts as an E3 ligase for TopBP1 and enhances ATR signaling, pharmacological inhibition of PHRF1's mono-ubiquitination activity or its interaction with TopBP1 could represent a novel therapeutic strategy for cancer. Replication stress is a well-known vulnerability in cancer cells, and targeting the proteins that regulate this process, such as PHRF1, could selectively sensitize tumor cells to DNA-damaging agents. Moreover, combining such inhibitors with traditional chemotherapy or targeted therapies could improve treatment efficacy by further disrupting the DDR in cancer cells while sparing normal cells.

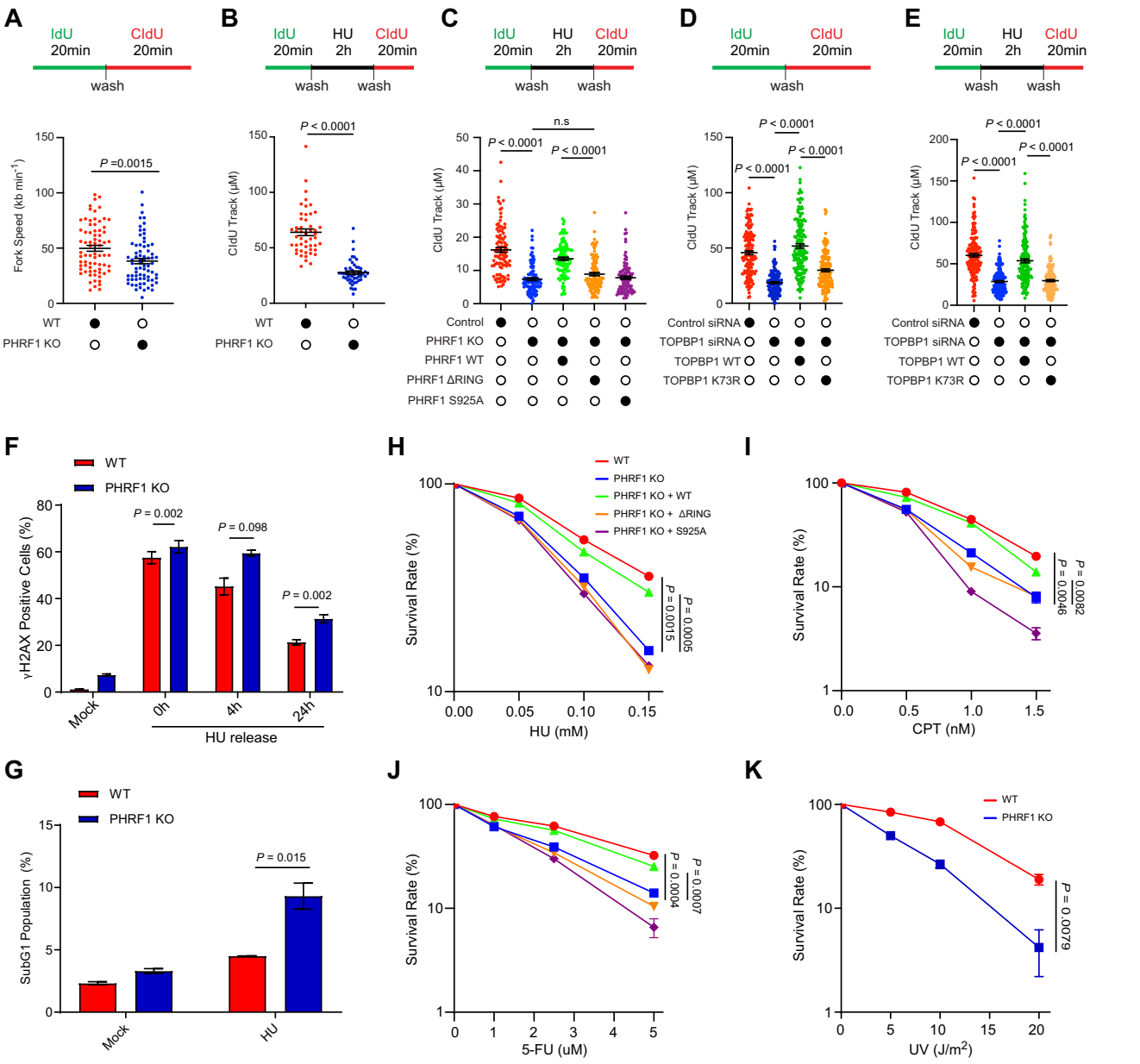

Figure 6. PHRF1 promotes stalled replication fork restart by ubiquitinating TopBP1. (**A**–**E**) WT or PHRF1 knockout HCT116 cells were transfected with the indicated vectors or siRNAs. 48 h later, cells were labeled with 25 μM IdU, followed by 200 μM CldU in each experiment. Cells were incubated with IdU for 20 min and then treated either with vehicle in panels (A, D) or 4 mM HU in panels (B, C, and E) for 2 h. After incubation, cells were labeled with CldU for 20 min. DNA fibers were stretched on a microscope slide, stained with IdU and CldU antibodies, and imaged. Fork speed was determined by measuring the length of the CldU track in panels (A, D) ($n = 100$). Stalled replication fork restart was assessed by measuring the length of the CldU track in panels (B, C, and E) ($n = 100$). (**F**, **G**) PHRF1 knockout or WT HCT116 cells were treated with 2 mM HU for 24 h, followed by release at the indicated times. Cells were collected, and γH2AX-positive in panel (F) and subG1 population (an indicator of cell death) in panel (G) were determined by flow cytometry. (**H**–**K**) PHRF1 knockout or WT HCT116 cells were transfected with the indicated vectors and then seeded into 6-well plates. Cells were treated with the indicated doses of HU (H), CPT (I), 5-FU (J), or UV (K). After 14 days, colony formation was assessed and the number of colonies was counted. The graphs represent mean ± standard error of mean, two-tailed, unpaired *t*-test; $n = 3$ independent experiments.

Our results also raise several important questions for future investigation. Specifically, the precise mechanisms underlying PHRF1 recruitment to stalled replication forks, particularly the role of histone methylation, warrant further exploration. While our *in vitro* binding assays demonstrate that PHRF1 binds to both H3K9me3 and H3K36me3, we observed that H3K36 methylation does not change at stalled replication forks under chaetocin treatment, and global H3K36me3 levels remain unaffected by prolonged chaetocin exposure. Interestingly, the Esashi group has reported that H3K36 methylation is regulated by SETD2 during replication stress [35], while Chang's group has shown that PHRF1 recognizes H3K36me3 in the context of nonhomologous end joining [20]. These findings suggest that H3K36 methylation may have a more complex role in DDR. Further studies are needed to clarify the role of H3K36 methylation in replication stress responses. Additionally, given the frequent crosstalk between different histone modifications, the role of histone methylation in regulating replication stress may be more intricate than currently understood.

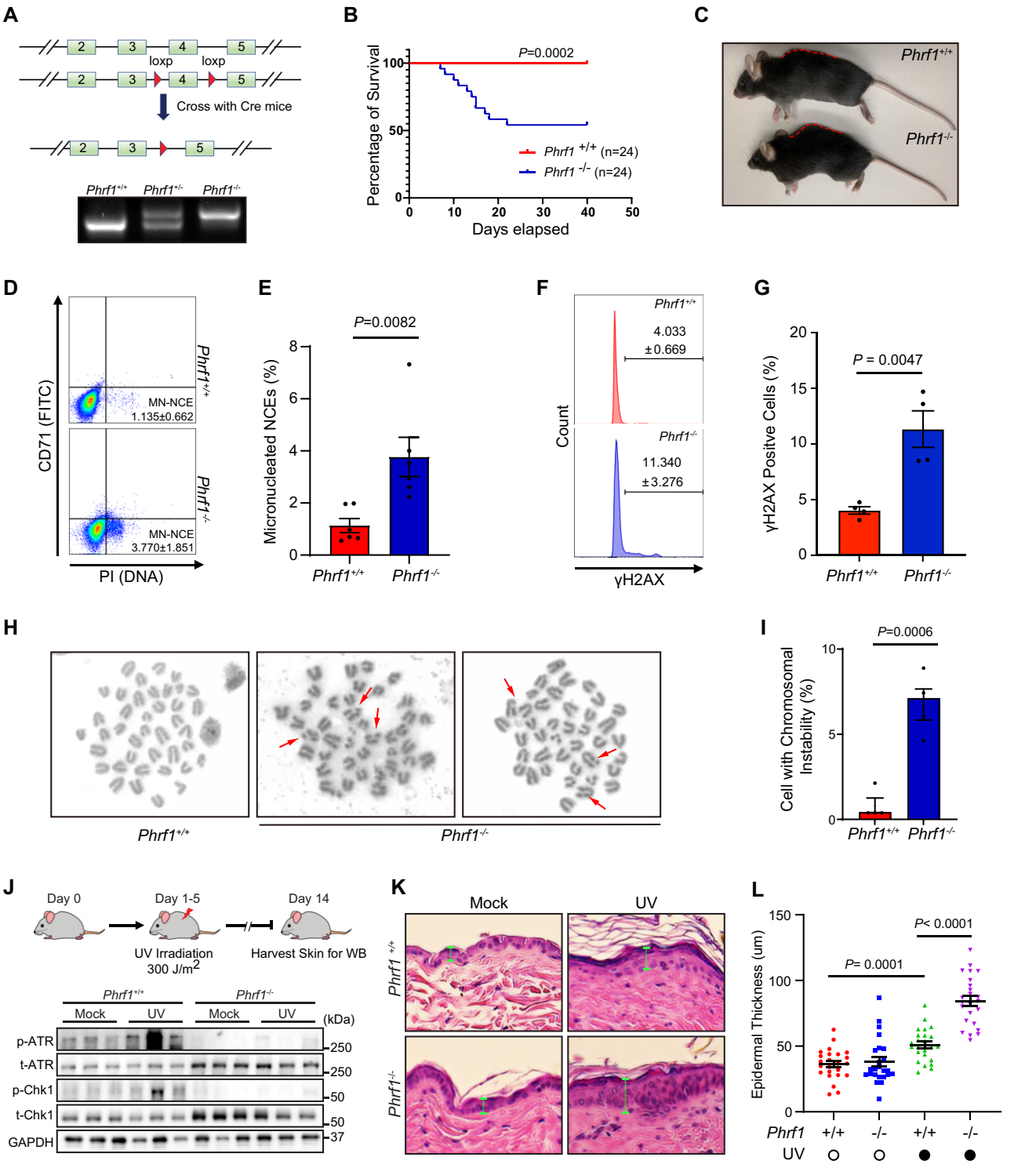

Figure 7. PHRF1 maintains genomic stability *invivo*. Generation and characterization of *Phrf1* knockout mice. (**A**) Schematic representation of WT and Cre/lox alleles in the *Phrf1* genomic locus. PCR analysis of genomic DNAs from $Phrf1^{+/+}$, $Phrf1^{+/-}$, and $Phrf1^{-/-}$ mice. (**B**, **C**) Phenotype of $Phrf1^{+/+}$ and $Phrf1^{-/-}$ mice. The number of surviving pups within 40 days after birth was assessed ($P = 0.0002$, Log rank test and Gehan–Breslow–Wilcoxon test) (B), and the $Phrf1^{-/-}$ mice displayed a hunched back phenotype compared to $Phrf1^{+/+}$ mice (C). (**D–I**) Genomic stability was examined by measuring the percentage of micronucleated normochromic erythrocytes (Mn-NCEs, $CD71^{-}PI^{+}$) in panels (D, E), γH2AX-positive splenocyte in panels (F, G), and thymocytes with chromosome breaks in panels (H, I). $n = 4$ independent experiments. Three mice per genotype. (**J, K**) Mice were irradiated with 300 J/m^2 UV daily for 5 days. After 14 days, ATR signaling was analyzed in skin tissues (**J**). Epidermal thickness was evaluated using H&E staining (K). (**L**) The graphs represent mean ± standard error of mean, two-tailed, unpaired *t*-test. $n \geq 3$ independent experiments. Three mice per genotype.

Additionally, understanding whether PHRF1's mono-ubiquitination of TopBP1 is the only or dominant mechanism for enhancing ATR activation, or whether there are additional substrates involved, could provide a more comprehensive understanding of PHRF1's role in DNA replication stress responses.

In conclusion, our findings establish PHRF1 as a key regulator of ATR signaling, functioning as an E3 ligase for TopBP1 to promote the replication stress response and maintain genomic stability. By identifying PHRF1 as a crucial player in ATR efficient activation, our study not only advances the understanding of replication stress responses but also suggests new avenues for therapeutic intervention in cancer.

Acknowledgements

We thank Dr Junjie Chen for kindly sharing the PHRF1 and TopBP1 constructs. The graphic abstract created in BioRender. Xiang, Y. (2025) https://BioRender.com/b88f892 and Fig. 2F created in BioRender. Chenghui, C. (2025) https://BioRender.com/r26o549.

Author contributions: F.Z., W.K., C.C., J.M., G.C., S.Q., and Y.H. designed and conducted experiments, analyzed data, and wrote the paper; S.Q., H.G., T.L. performed bioinformatics data; W.K., F.Z. and Z.L. Conceptualization, Writing-review & editing, Supervision, Project administration, Funding acquisition. All authors have read and agreed to the published version of the manuscript.

Supplementary data

Supplementary data is available at NAR online.

Conflict of interest

None declared.

Funding

This research was supported by the Mayo Foundation, the National Natural Science Foundation of China (32370779), the Provincial Natural Science Foundation of Hunan (2024JJ3008), the National Research Foundation of Korea (NRF) grants (2022R1A2C1091563, 2019M3E5D3073092), and the Soonchunhyang University Research Fund. Additionally, this research was supported by the Brain Pool program, funded by the Ministry of Science and ICT through the National Research Foundation of Korea (RS-2023-00218261). Funding to pay the Open Access publication charges for this article was provided by National Research Foundation of Korea (NRF) (2022R1A2C1091563).

Data availability

All data are available upon request (wootaek@sch.ac.kr).

References

1. Gaillard H, Garcia-Muse T, Aguilera A. Replication stress and cancer. *Nat Rev Cancer* 2015;**15**:276–89. https://doi.org/10.1038/nrc3916
2. Burrell RA, McClelland SE, Endesfelder D *et al.* Replication stress links structural and numerical cancer chromosomal instability. *Nature* 2013;**494**:492–6. https://doi.org/10.1038/nature11935
3. Zou Y, Liu Y, Wu X *et al.* Functions of human replication protein A (RPA): from DNA replication to DNA damage and stress responses. *J Cell Physiol* 2006;**208**:267–73. https://doi.org/10.1002/jcp.20622
4. Cortez D. Preventing replication fork collapse to maintain genome integrity. *DNA Repair (Amst)* 2015;**32**:149–57. https://doi.org/10.1016/j.dnarep.2015.04.026
5. Zou L, Liu D, Elledge SJ. Replication protein A-mediated recruitment and activation of Rad17 complexes. *Proc Natl Acad Sci USA* 2003;**100**:13827–32. https://doi.org/10.1073/pnas.2336100100
6. Wang X, Zou L, Lu T *et al.* Rad17 phosphorylation is required for claspin recruitment and Chk1 activation in response to replication stress. *Mol Cell* 2006;**23**:331–41. https://doi.org/10.1016/j.molcel.2006.06.022
7. Rauen M, Burtelow MA, Dufault VM *et al.* The human checkpoint protein hRad17 interacts with the PCNA-like proteins hRad1, hHus1, and hRad9. *J Biol Chem* 2000;**275**:29767–71. https://doi.org/10.1074/jbc.M005782200
8. Zou L, Elledge SJ. Sensing DNA damage through ATRIP recognition of RPA–ssDNA complexes. *Science* 2003;**300**:1542–8. https://doi.org/10.1126/science.1083430
9. Cotta-Ramusino C, McDonald ER 3rd, Hurov K *et al.* A DNA damage response screen identifies RHINO, a 9-1-1 and TopBP1 interacting protein required for ATR signaling. *Science* 2011;**332**:1313–17. https://doi.org/10.1126/science.1203430
10. Kim W, Zhao F, Wu R *et al.* ZFP161 regulates replication fork stability and maintenance of genomic stability by recruiting the ATR/ATRIP complex. *Nat Commun* 2019;**10**:5304. https://doi.org/10.1038/s41467-019-13321-z
11. Haahr P, Hoffmann S, Tollenaere MA *et al.* Activation of the ATR kinase by the RPA-binding protein ETAA1. *Nat Cell Biol* 2016;**18**:1196–207. https://doi.org/10.1038/ncb3422
12. Bass TE, Luzwick JW, Kavanaugh G *et al.* ETAA1 acts at stalled replication forks to maintain genome integrity. *Nat Cell Biol* 2016;**18**:1185–95. https://doi.org/10.1038/ncb3415
13. Lee YC, Zhou Q, Chen J *et al.* RPA-binding protein ETAA1 is an ATR activator involved in DNA replication stress response. *Curr Biol* 2016;**26**:3257–68. https://doi.org/10.1016/j.cub.2016.10.030
14. Frattini C, Promonet A, Alghoul E *et al.* TopBP1 assembles nuclear condensates to switch on ATR signaling. *Mol Cell* 2021;**81**:1231–45. https://doi.org/10.1016/j.molcel.2020.12.049
15. Cortez D, Guntuku S, Qin J *et al.* ATR and ATRIP: partners in checkpoint signaling. *Science* 2001;**294**:1713–16.https://doi.org/10.1126/science.1065521
16. Bigot N, Day M, Baldock RA *et al.* Phosphorylation-mediated interactions with TOPBP1 couple 53BP1 and 9-1-1 to control the G1 DNA damage checkpoint. *eLife* 2019;**8**:e44353. https://doi.org/10.7554/eLife.44353
17. Liu T, Lin YH, Leng W *et al.* A divergent role of the SIRT1-TopBP1 axis in regulating metabolic checkpoint and DNA damage checkpoint. *Mol Cell* 2014;**56**:681–95. https://doi.org/10.1016/j.molcel.2014.10.007
18. Kim W, Zhao F, Gao H *et al.* USP13 regulates the replication stress response by deubiquitinating TopBP1. *DNA Repair (Amst)* 2021;**100**:103063. https://doi.org/10.1016/j.dnarep.2021.103063
19. Honda Y, Tojo M, Matsuzaki K *et al.* Cooperation of HECT-domain ubiquitin ligase hHYD and DNA topoisomerase II-binding protein for DNA damage response. *J Biol Chem* 2002;**277**:3599–605. https://doi.org/10.1074/jbc.M104347200
20. Chang CF, Chu PC, Wu PY *et al.* PHRF1 promotes genome integrity by modulating non-homologous end-joining. *Cell Death Dis* 2015;**6**:e1716. https://doi.org/10.1038/cddis.2015.81
21. An CH, Son HJ, Yoo NJ *et al.* Downregulation of a putative tumor suppressor gene PHRF1 in gastric and colorectal cancers. *Pathol Res Pract* 2020;**216**:152984. https://doi.org/10.1016/j.prp.2020.152984
22. Ettahar A, Ferrigno O, Zhang MZ *et al.* Identification of PHRF1 as a tumor suppressor that promotes the TGF-beta cytostatic program through selective release of TGIF-driven PML

inactivation. *Cell Rep* 2013;**4**:530–41. https://doi.org/10.1016/j.celrep.2013.07.009
23. Prunier C, Zhang MZ, Kumar S *et al.* Disruption of the PHRF1 tumor suppressor network by PML-RARα drives acute promyelocytic leukemia pathogenesis. *Cell Rep* 2015;**10**:883–90. https://doi.org/10.1016/j.celrep.2015.01.024
24. Knijnenburg TA, Wang L, Zimmermann MT *et al.* Genomic and molecular landscape of DNA damage repair deficiency across The Cancer Genome Atlas. *Cell Rep* 2018;**23**:239–54. https://doi.org/10.1016/j.celrep.2018.03.076
25. Marquard AM, Eklund AC, Joshi T *et al.* Pan-cancer analysis of genomic scar signatures associated with homologous recombination deficiency suggests novel indications for existing cancer drugs. *Biomark Res* 2015;**3**:9. https://doi.org/10.1186/s40364-015-0033-4
26. Sirbu BM, Couch FB, Cortez D. Monitoring the spatiotemporal dynamics of proteins at replication forks and in assembled chromatin using isolation of proteins on nascent DNA. *Nat Protoc* 2012;**7**:594–605. https://doi.org/10.1038/nprot.2012.010
27. Kawasaki A, Furukawa H, Kondo Y *et al.* Association of PHRF1-IRF7 region polymorphism with clinical manifestations of systemic lupus erythematosus in a Japanese population. *Lupus* 2012;**21**:890–95. https://doi.org/10.1177/0961203312439333
28. Dungrawala H, Cortez D. Purification of proteins on newly synthesized DNA using iPOND. *Methods Mol Biol* 2015;**1228**:123–31. https://doi.org/10.1007/978-1-4939-1680-1_10
29. Musselman CA, Kutateladze TG. Handpicking epigenetic marks with PHD fingers. *Nucleic Acids Res* 2011;**39**:9061–71. https://doi.org/10.1093/nar/gkr613
30. Feng G, Yuan Y, Li Z *et al.* Replication fork stalling elicits chromatin compaction for the stability of stalling replication forks. *Proc Natl Acad Sci USA* 2019;**116**:14563–72. https://doi.org/10.1073/pnas.1821475116
31. Oeck S, Malewicz NM, Krysztofiak A *et al.* High-throughput Evaluation of Protein Migration and Localization after Laser Micro-Irradiation. *Sci Rep* 2019;**9**:3148–48. https://doi.org/10.1038/s41598-019-39760-8
32. Matsumura Y, Ananthaswamy HN. Molecular mechanisms of photocarcinogenesis. *Front Biosci* 2002;**7**:D765–83. https://doi.org/10.2741/matsumur
33. El-Abaseri TB, Putta S, Hansen LA. Ultraviolet irradiation induces keratinocyte proliferation and epidermal hyperplasia through the activation of the epidermal growth factor receptor. *Carcinogenesis* 2006;**27**:225–31. https://doi.org/10.1093/carcin/bgi220
34. Vind AC, Wu Z, Firdaus MJ *et al.* The ribotoxic stress response drives acute inflammation, cell death, and epidermal thickening in UV-irradiated skin *in vivo*. *Mol Cell* 2024; **84**:4774–89. https://doi.org/10.1016/j.molcel.2024.10.044
35. Bleuyard JY, Fournier M, Nakato R *et al.* . MRG15-mediated tethering of PALB2 to unperturbed chromatin protects active genes from genotoxic stress. *Proc Natl Acad Sci U S A* 2017;**114**:7671–6. https://doi.org/10.1073/pnas.1620208114

Received: March 12, 2024. **Revised:** December 28, 2024. **Editorial Decision:** January 20, 2025. **Accepted:** January 28, 2025